Collimation of electrons at closed magnetic barriers in two-dimensional electron gases

M. Cerchez,[*] T. Chirila,[†] H. Bettermann,[‡] B. Schüler,[†] and T. Heinzel[§]
Condensed Matter Physics Laboratory, Heinrich-Heine-Universität, D-40204 Düsseldorf, Germany

(Received 8 October 2018; published 11 February 2019)

It is shown that closed magnetic barriers defined in two-dimensional electron gases generate a collimated emerging electron beam at the edge of the Hall bar. The collimation takes place through two mechanisms: electron selection for $\vec{E} \times \vec{B}$ drift at the edge and bulk collimation of the emerging electrons due to the magnetic field gradient. The collimation effect is verified by experiments and simulations: a second magnetic barrier used as a probe will reflect the collimated beam differently when positioned at various distances from the first one, resulting in oscillations in the resistance.

DOI: 10.1103/PhysRevB.99.085303

I. INTRODUCTION

Two-dimensional electron gases (2DEGs) with large mobilities enable the implementation of ballistic circuits and devices. For example, ballistic rectification at asymmetric Hall crosses [1] and the quantization of the conductance in quasi-one-dimensional ballistic wires [2,3] have been demonstrated. Two prominent members of the family of electron ballistics are collimation and focusing. The electron beam emerging from a quantum point contact is typically collimated [4,5]. Electrostatic lenses [6] and elliptic reflectors [7] are based on gated nanostructures that change the electron trajectories and allow electron focusing. Coherent electron focusing with quantum point contacts in a 2DEG exposed to a homogeneous magnetic field was demonstrated by van Houten *et al.* [8].

One structural element of ballistic electronic circuits in 2DEGs is a magnetic barrier [9]. This term usually designates a magnetic field configuration which is localized in the longitudinal direction and homogeneous in the transverse direction with respect to the flow of electrons. Magnetic barriers have been at the focus of various experimental and theoretical studies in relation to classical transport properties [10–19], magnetic confinement in both semiconductor heterostructures [20–22], resonant reflection [23], Hall magnetometry [24], and spin filtering in nanostructures [25–30]. Furthermore, magnetic barriers appear as structural elements in magnetic superlattices [9,31–33]. Finally, we mention the relevance of magnetic textures for graphene, where not only can electronic confinement be achieved by applying inhomogeneous magnetic fields [34,35] but also mechanical strain can cause a modification of the hopping matrix elements between the electronic sites, an effect that can be mapped onto an effective magnetic field [36], with values as large as 300 T [37].

Here, we show that, in an implementation which is typical for two-dimensional electron gases in Ga[Al]As heterostructures, magnetic barriers can collimate electron beams. Above a critical magnetic barrier amplitude and in the absence of additional scattering, all electrons that enter the barrier region sufficiently far away from the edge of the Hall bar get reflected by the Lorentz force. However, electrons close to the sample edge may experience an $\vec{E} \times \vec{B}$ drift and pass the barrier via skipping orbits. In this *closed regime*, the magnetic barrier thus forms a pointlike electron emitter. We show with numerical simulations how the emerging electron beam is collimated by the magnetic barrier, and the results are verified experimentally by studying the resistance of two magnetic barriers in series, where the second barrier, placed at various distances, acts as a probe for the collimated electron beam emerging from the first one. Resistance oscillations as a function of the distance between the two barriers are observed.

In Sec. II we present a study of the statistics of the electron flow emerging at the edge of the magnetic barrier, while in Sec. III we present an example of the effects produced by the collimation on the resistance, experimentally and with simulations. The paper closes with a summary of the results and our conclusions (Sec. IV).

II. STATISTICS OF ELECTRON COLLIMATION AT A CLOSED MAGNETIC BARRIER

The usual method for defining a magnetic barrier in a 2DEG is by placing a ferromagnetic stripe on the surface of the host semiconductor heterostructure and magnetizing it in the direction parallel to the applied current [x direction in Fig. 1(a)]. The component of the fringe field perpendicular to the 2DEG (z direction) has a peaked shape, with its maximum beneath the edge of the stripe, and, assuming that the ferromagnet has a very large extension in the y direction, may be expressed as [15]

$$B_z(x) = -\frac{B_s}{4\pi} \ln\left[\frac{x^2 + d^2}{x^2 + (d+h)^2}\right], \tag{1}$$

where $B_s = \mu_0 M$ is the product of the vacuum permeability and the magnetization, h is the thickness of the ferromagnetic

[*]Corresponding author: mihai.cerchez@hhu.de
[†]Present address: Infineon Technologies AG, Am Campeon 1-15, 85579 Neubiberg, Germany.
[‡]Present address: Asphericon GmbH, Stockholmer Strasse 9, 07747 Jena, Germany.
[§]http://www.solid-state-physics.hhu.de/

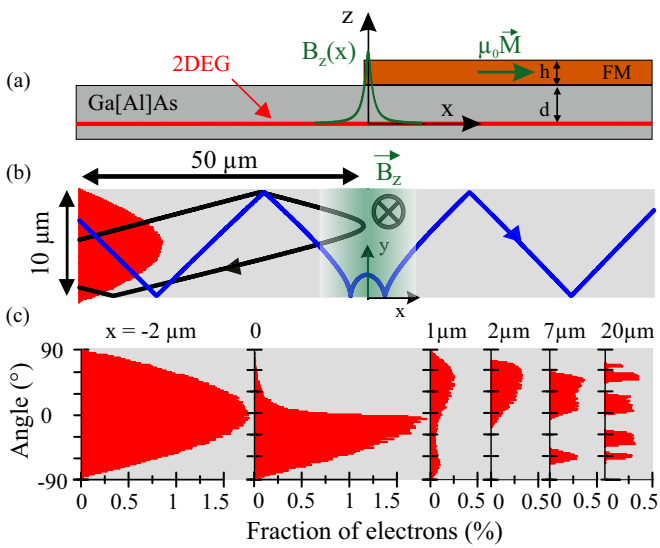

FIG. 1. (a) Cross section of the considered implementation of a magnetic barrier $B_z(x)$ in a 2DEG. (b) Ballistic electrons may pass through a closed magnetic barrier in skipping orbits at the edge (blue transmitted electron trajectory). In the bulk, electrons get reflected by the closed barrier (black electron trajectory). The initial cosine distribution is indicated on the left side of the Hall bar. (c) Distribution of angles of electron velocity with respect to the x direction at different distances from the center of the magnetic barrier at $x = 0$. The bin size of the histogram is 2°.

stripe, and d denotes the depth of the 2DEG below the sample surface. The full width at half maximum is $2\sqrt{d(d+h)}$ and is of the order of 300 nm in typical samples [14,15,18,19]. The x component of the fringe field produces weak effects and will be neglected below. For an infinitely extended 2DEG with no scattering in the magnetic barrier region, the electrons approaching the barrier will be deflected by the Lorentz force, and if the magnetic barrier is high enough, none of the electrons may pass through, leading to an infinite resistance. However, the resistance is limited by edge skipping [18] in the magnetic barrier region. The edge skipping is unidirectional at each edge, and an asymmetry is induced in the distribution of the velocity vector angles (which from now on we will call *the distribution*) that the transmitted electrons have with respect to the x direction. To study the distribution, we simulated the electron flow by injecting 10^6 electrons in a Hall bar of 10 μm at a distance of 50 μm in front of the magnetic barrier [Fig. 1(b)] given by Eq. (1). We use the values $d = 65$ nm, $h = 250$ nm, and the electron density $n = 2.45 \times 10^{15}\,\mathrm{m}^{-2}$. B_s is set to 1.5 T, which provides a maximum barrier height of $B_z(0) = 0.38$ T. These values are in agreement with the experimental ones that will be discussed below. We calculate the electron trajectories by solving the semiclassical equations of motion in the presence of the magnetic field given by Eq. (1) in combination with hard electrostatic walls at $y = 0$ and 10 μm, which simulate the edges of the Hall bar, and we record the distribution. The initially injected electrons have a cosine distribution to reflect the electron injection rate [38].

In Fig. 1(c), we show the distribution (+90° is along the y axis, and 0° is along the x axis) at various positions along the x axis. We characterize the distribution by its mean value $\overline{\alpha}$ and its standard deviation σ_α. The center of the magnetic barrier is at $x = 0$ [Fig. 1(b)]. At $x = -2\,\mu$m, the initial cosine distribution is almost completely preserved [Fig. 1(c)], with an average angle of $\overline{\alpha} = -0.08°$ and $\sigma_\alpha = 39°$ (for the initially injected cosine distribution, the value is $\sigma_\alpha^{cos} = 39.1°$). One hundred percent of the injected electrons reach this point. However, only 54% of the electrons reach the position $x = 0$. The distribution at this point is asymmetric, as many electrons approaching the barrier at negative angles [e.g., the black electron trajectory in Fig. 1(b)] were already reflected by the barrier, while many electrons that approached the barrier at a positive angle are deflected into a negative angle by the time they reach $x = 0$. About 9.9% of the electrons reach the position $x = 1\,\mu$m [third histogram in Fig. 1(c)], where the angles have shifted to more positive values, since electrons get reflected at the lower edge of the Hall bar [the blue trajectory of a transmitted electron in Fig. 1(b) is an example]. At $x = 2\,\mu$m, most of the electrons that passed through the barrier experienced a reflection at the lower edge, and a very small tail of the distribution is still present at negative angles close to zero, corresponding to electrons moving almost parallel to the lower sample edge. At $x = 7\,\mu$m, the distribution splits into two well-separated peaks. The peak at negative angles represents electrons that were reflected at the upper Hall bar edge. As we move to larger x coordinates, the number of peaks in the distribution increases due to successive reflections at the edges. These snapshots also show that directly after passing the magnetic barrier, the distribution gets narrower, which corresponds to a collimation of the electron beam. In order to characterize this effect further, the *angle maps*, i.e., the local average velocity vector angles of the electrons α as a function of x and y, are shown as color plots in Fig. 2 for three different values of B_s. For the given electron density, the critical value of the saturation magnetization at which the magnetic barrier is closed in the absence of edges is $B_{sc} = 1.32$ T. Also shown are the corresponding mean $\overline{\alpha}(x)$ and standard deviation $\sigma_\alpha(x)$ of the distribution, as well as the average $\overline{y}(x)$ and the standard deviation $\sigma_y(x)$ of the y position of the electrons. No electron trajectories are recorded in the white area denoted as the no trajectory area (NTA).

As the magnetic barrier height increases, the angle maps indicate that electrons pass only at the lower edge, and the maximum angle of emerging electrons decreases with larger magnetization, resulting in a collimated electron flow with a narrower distribution. The maximum angle in the map decreases from 67.7° at $B_s = 1.5$ T to 42.8° at $B_s = 2.0$ T and to 27.4° at $B_s = 2.5$ T. As the electron beam hits the upper edge of the Hall bar, specular reflections lead to a homogenization of the distribution on a length of about $x = 30\,\mu$m in the x direction, with $\overline{y}$ approaching 5 μm, the center of the Hall bar, and $\overline{\alpha}$ approaching zero.

We look in some more detail at the case of $B_s = 1.5$ T in Fig. 2(a). First of all, $\sigma_\alpha(1.5\,\mathrm{T})$ has a minimum around $x = 0$, followed by a sharp maximum at 0.8 μm. The maximum is due to the reflection of the electron beam at the lower edge, with a maximum disorder when half is reflected and moving upwards while the other half is still moving downwards, also indicated by the fact that $\overline{\alpha} = 0$ at the position where σ_α has a maximum. For x between 0.8 and 4.2 μm, $\overline{\alpha}$ decreases

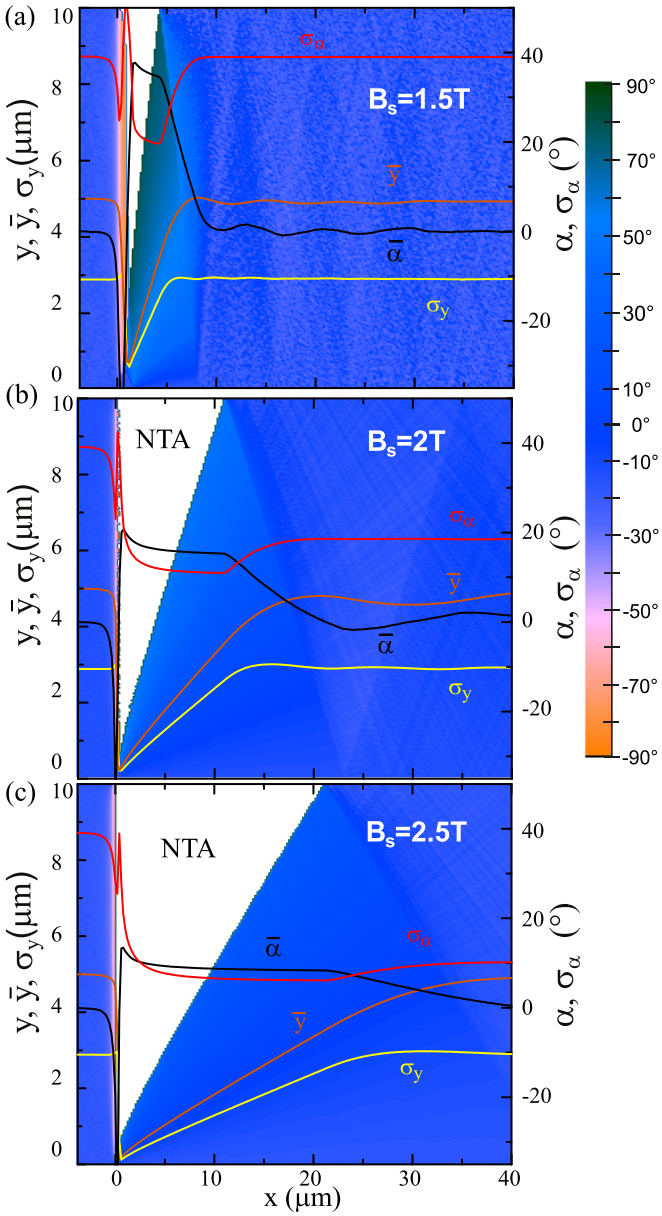

FIG. 2. Average velocity angle $\bar{\alpha}$ and its standard deviation σ_α, as well as the average y position $\bar{y}$ of the electrons and its standard deviation σ_y for three values of B_s. The background color plot represents the local average angle of the electrons within the Hall bar according to the color code to the right, from $x = -4$ to 40 μm. NTA denotes the area (white) where no electron trajectories are recorded and is not part of the color scale.

monotonically to $\bar{\alpha}(1.5\,\mathrm{T}, 4.2\,\mu\mathrm{m}) = 34.6°$. Simultaneously, σ_α decreases to a minimum of 19.6° at $x = 4.2\,\mu$m. As the first electrons of this beam, traveling at large angles, hit the upper edge, σ_α starts to increase and reaches its original value of ≈39° at around $x = 10\,\mu$m.

For larger values of the magnetization [Figs. 2(b) and 2(c)], the collimation is stronger, which may be observed in the decreasing $\bar{\alpha}$ and increased NTA. For example, the minimum standard deviation for $B_s = 2.0\,\mathrm{T}$ is $\sigma_\alpha(2.0\,\mathrm{T}, 10.9\,\mu\mathrm{m}) = 11.1°$, and the minimum average angle is $\bar{\alpha}(2.0\,\mathrm{T}, 10.9\,\mu\mathrm{m}) = 15.2°$, while the corresponding

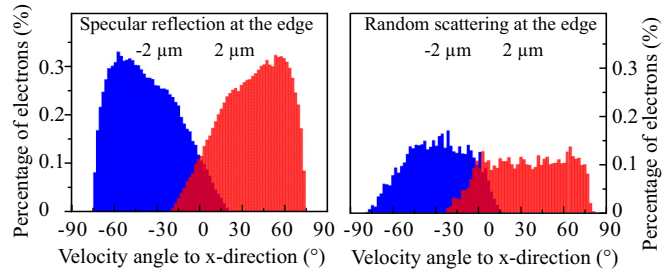

FIG. 3. The distribution of emerging electrons at 2 μm and their corresponding distribution at $-2\,\mu$m for specular reflection at the lower edge (left) and random scattering at the lower edge (right).

minima for $B_s = 2.5\,\mathrm{T}$ are $\sigma_\alpha(2.5\,\mathrm{T}, 21.4\,\mu\mathrm{m}) = 6.12°$ and $\bar{\alpha}(2.5\,\mathrm{T}, 21.4\,\mu\mathrm{m}) = 8.32°$, respectively.

These simulations show that the strength of the magnetic barrier field gradient in the closed regime determines the degree of collimation of the transmitted electron beam by two mechanisms. Inside the barrier, the collimation takes place through $\vec{E} \times \vec{B}$ drift, and behind the barrier, it is due to the magnetic field gradient. As seen in Figs. 2(b) and 2(c), the emerging beam collimation after the $\vec{E} \times \vec{B}$ drift is stronger for higher barriers. In the left panel of Fig. 3, the distribution at $x = 2\,\mu$m in the case of a ballistic system with specular reflection at the lower edge is shown (in red). As expected from time-reversal symmetry arguments, under the reversal of the directions of the current and the magnetic field, we will obtain a symmetric distribution with respect to the case described above. This means that the distribution of the emerging electrons at $x = 2\,\mu$m must originate from a symmetric distribution at $x = -2\,\mu$m. This is also represented (blue) in the left panel of Fig. 3. The distribution is mirrored in the following way: the electrons entering at large (small) angles may emerge at small (large) angles depending on the initial position and angle, which also determines how many times an electron is reflected at the lower edge during skipping. This indicates directly that a narrow emerging distribution comes from a symmetrically narrow incident distribution. This happens because for larger magnetic fields, only electrons that are closer to the lower edge and moving at larger angles will pass through the $\vec{E} \times \vec{B}$ drift. After emerging at the lower edge but still in the magnetic field gradient, the electrons that move towards the upper edge at larger angles will spend more time in the magnetic barrier region until they reach the same x position, and therefore, they will be deflected more than the electrons that move more parallel to the sample lower edge, improving the collimation. Thus, the collimation of the electron beam emerging at the lower edge at an average angle $\bar{\alpha} > 0$ and the shape of the magnetic barrier are correlated. Even though a specific shape of the magnetic barrier has been assumed here, the effect is more universal since it requires just a magnetic barrier with smooth edges.

III. EFFECTS OF COLLIMATION ON THE RESISTANCE OF CLOSED DOUBLE MAGNETIC BARRIERS

It is to be expected that the collimation of the electron beam emerging at the lower edge of the magnetic barrier will have influence on the resistance of a ballistic device, or, in more

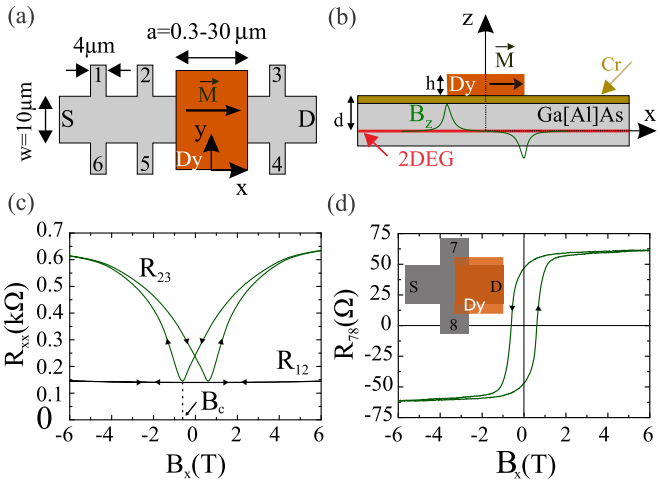

FIG. 4. (a) Schematic top view of the sample, with the relevant geometrical parameters. (b) The corresponding cross-sectional view with the x-dependent magnetic field profile at the 2DEG depth, showing two magnetic barriers of opposite polarity under the edges of the stripe, as described by Eq. (2). (c) The magnetoresistance R_{23} produced by the magnetic stripe as a function of the applied magnetic field and the background resistance R_{12} of the Hall bar. (d) Hysteresis in the Hall resistance $R_{78}(B)$ measured under a single edge of a ferromagnetic stripe with $a = 40\,\mu$m, where one edge is at the center of a Hall cross.

general terms, for samples where the distance between the magnetic barrier and the point where the electron beam hits the upper edge of the Hall bar is smaller than the mean free path of the electrons. One straightforward way to detect the emerging electron beam is by using a second, closed magnetic barrier which acts as a probe. A ferromagnetic stripe of finite extension on top of the sample generates two magnetic barriers in series of equal strength but of opposite polarity [see the sketch in Figs. 4(a) and 4(b)]. If the edge transmission of the collimating magnetic barrier placed at $x = 0$ occurs at the lower edge ($y = 0$), the electrons can pass the probe, the second barrier, only at the upper edge ($y = w$). Thus, if the probe barrier is placed at the position where the collimated electron beam hits the upper edge, we expect a resistance minimum, while the resistance should be particularly large for a probe position where $\bar{y}$ is at the center of the Hall bar. Consequently, the resistance of the closed magnetic barriers in series should show a characteristic dependence on the spacing a between them. The magnetic field as a function of x for this configuration reads

$$B_z(x) = -\frac{B_s}{4\pi}\left\{\ln\left[\frac{x^2+d^2}{x^2+(d+h)^2}\right] - \ln\left[\frac{(x-a)^2+d^2}{(x-a)^2+(d+h)^2}\right]\right\}. \quad (2)$$

The layout of the samples is shown in Figs. 4(a) and 4(b). We used a commercially available $GaAs/Al_{0.3}Ga_{0.7}As$ heterostructure with a 2DEG located at $d = 65$ nm below the surface, from which we prepared ten identical Hall bars by optical lithography and wet-chemical etching. The width of the Hall bars is 10 μm. The 2DEG has an electron density of $n = 2.45 \times 10^{15}\,\mathrm{m}^{-2}$ and a mobility of $\mu = 32\,\mathrm{m}^2/\mathrm{V\,s}$, providing a mean free path of 2.6 μm, at a temperature of 1.4 K. Ferromagnetic Dy stripes with a thickness of $h = 250$ nm and various lengths a, which define the spacing between the collimating (first) barrier and the probe (second) barrier, were deposited simultaneously on the Hall bars by sublimation of Dy in high vacuum (on top of a Cr layer 2 nm thick, which limits the piezoelectric strain under the Dy edge). The Dy stripes extend over a large distance outside the Hall bar. The samples were finally covered by Cr/Au gates to prevent Dy oxidation, and the surface metals were grounded during the experiments.

Nine stripes with lengths $a = 0.35, 0.7, 1.3, 2.2, 3.1, 4, 7.1, 7.2$, and 30 μm are prepared. They were positioned between probes 2 and 3, which were used to measure the voltage drop across the two barriers formed under the two edges of each stripe in a four-probe geometry [Fig. 4(a)] and represented as the magnetoresistance R_{23} vs the applied magnetic field B_x, an example of which is shown in Fig. 4(c). The magnetoresistance of the 2DEG between voltage probes 2 and 3 in the absence of magnetic barriers $R_{23}(B_c)$ is determined from the minimum of $R_{23}(B_x)$ at the coercive field of the Dy stripe B_c. When the mobility and electron density in the 2DEG are not modified by the presence of the Dy stripe, $R_{23}(B_c)$ equals $R_{12}(B_c)$ [as may be seen in Fig. 4(c)], where the later term is scaled to the same length. Finally, we are interested in the resistance change ΔR between the resistance when the stripes are fully magnetized (at a saturation field of 6 T) and the resistance when the stripes are demagnetized, $\Delta R = R_{23}(6\,\mathrm{T}) - R_{23}(B_c)$.

A tenth magnetic stripe has a length of 40 μm. The first edge resides in between two voltage probes, while the second one is placed at the center of a Hall cross [inset in Fig. 4(d)]. For this value of a, much larger than the mean free path, the two magnetic barrier resistances are additive. The measured Hall voltage as a function of B_x is used to determine the saturation magnetization of the stripe [24,39], which is found to be 1.5 T, and the longitudinal resistance measurement across the second magnetic barrier is used to determine the magnetoresistance of an individual barrier. All magnetoresistance measurements were carried out in a liquid-helium cryostat with a base temperature of 1.4 K using a lock-in technique with a current of $I = 100$ nA at 17.7 Hz.

The measured values for $\Delta R(a)$ are shown in Fig. 5. At very small values of a, $\Delta R(a)$ tends to zero. A maximum in the resistance is visible at $a = 3.1\,\mu$m, with a value that exceeds twice the value of a single magnetic barrier (indicated by the red horizontal line). Also, a minimum at 7.1 μm is observed. For larger distances, the resistance increases and saturates towards 30 μm at a value which equals twice the resistance of a single barrier.

In order to obtain a better understanding of this behavior, we simulated the resistance of the 2DEG produced by such a stripe, using the Landauer-Büttiker formalism [40] in a four-probe geometry in the ballistic limit [41]; 10^6 electrons are injected from each contact using a cosine distribution. The injection line is at 50 μm before the first magnetic barrier, and the electron trajectories are calculated solving the semiclassical differential equations of motion in the presence of the inhomogeneous magnetic barrier, given by Eq. (2). The transmission probabilities between various contacts are

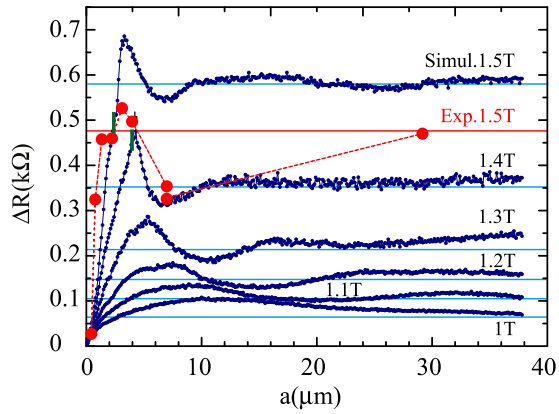

FIG. 5. Red circles: measured values of $\Delta R(a)$ of the two magnetic barriers in series. The dashed red line is a guide to the eye. The solid horizontal red line denotes the resistance of two individual magnetic barriers in series. The measured magnetization of the Dy stripe that formed the barriers was $B_s = 1.5\,\mathrm{T}$. Blue circles: simulations of $\Delta R(a)$ for various magnetizations between $B_s = 1.0\,\mathrm{T}$ and $B_s = 1.5\,\mathrm{T}$. The blue horizontal lines denote the corresponding resistances of two single barriers in series. Furthermore, for the B_s values where the magnetic barriers are closed at large a, the vertical green bars denote the separation at which the barriers open up, i.e., where bulk transmission is enabled.

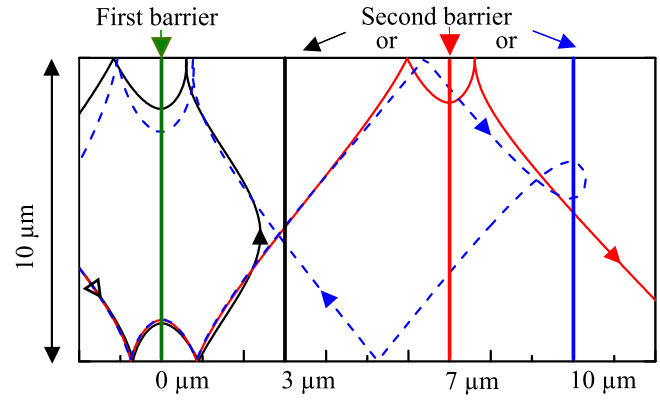

FIG. 6. The trajectory of an electron when the first barrier is positioned at (0 μm and the second barrier is positioned at 3, 7, or 10 μm.

translated into a conductance matrix [42], and thereby, the potential difference between different probes is calculated. Infinite potential walls at the edges of the Hall bar are considered, at which electrons experience specular reflection. No diffuse scattering is taken into account either at the edge or at impurities. The results of these simulations are presented in Fig. 5 as well. Each $\Delta R(a)$ trace (blue lines and dots) corresponds to one value of the magnetization, while a is varied in between 0 and 38 μm.

First of all, as a approaches zero, ΔR vanishes rapidly. This is due to the cancellation of the two magnetic barriers at small distances by reason of their opposite polarity. Due to this effect, magnetic barriers that are closed for large a open up at a critical separation as a is decreased. These critical separations are indicated by the vertical green bars in Fig. 5 for the uppermost two traces where the magnetic barriers are closed at large distances. Also, an oscillatory behavior of $\Delta R(a)$ is found in the simulations, which gets more pronounced as B_s increases. The peak value of the first maximum is well above the resistance expected for two individual magnetic barriers in series (these values are indicated by the horizontal blue lines). This peak occurs at separations where the electron beam emerging from the collimating barrier hits the probe barrier away from the transmissive upper edge of the Hall bar such that electrons are reflected with highest probability towards the upper edge of the collimating barrier, which allows transmission to the left. If the collimated electron beam hits the probe barrier away from the upper edge, the reflection probability at the probe barrier is higher than what the uncollimated electrons had at the collimating barrier. As the separation is increased by approximately a factor of 2, the electron beam hits the probe barrier at the upper edge of the Hall bar, where there is a high probability of transmission to the right. Therefore, ΔR drops below the resistance of two barriers in series. For example, Fig. 2(a) indicates that the electron beam exiting the first barrier has an x interval (1.8 to 4.4 μm) in which most electrons are moving upwards [$\overline{\alpha}(3.3\,\mu\mathrm{m}) = 35^\circ$] in a narrow beam $\sigma_\alpha(3.3\,\mu\mathrm{m}) = 20.2^\circ$, which is slightly more than half of the original cosine distribution. Moreover, most of the electrons are nearer to the lower edge than to the upper, transmissive one (i.e., $\overline{y}(3.3\,\mu\mathrm{m}) = 2.6\,\mu\mathrm{m}$) and in a quite narrow region ($\sigma_y(3.3\,\mu\mathrm{m}) = 1.8\,\mu\mathrm{m}$. This produces a scenario where the fraction of electrons that gets reflected by the second barrier reaches a maximum. In Fig. 6, we show the calculated possible trajectories of an electron passing in $\vec{E} \times \vec{B}$ drift through the first barrier and encountering the second barrier placed at three possible distances: 3 μm (near the maximum in resistance), 7 μm (near the minimum in resistance), and 10 μm. The second barrier in the 3-μm case reflects the electron directly into the first magnetic barrier at its upper edge that transports the electron back to the left contact. For the second barrier placed at a larger distance of 7 μm the electron reaches the upper edge in the second magnetic barrier region, and the second barrier is passed by $\vec{E} \times \vec{B}$ drift. Placing the second barrier farther away (10 μm) produces a reflection of the electron that travels back through the first barrier and into the left-hand contact. If the barrier were placed at a considerably smaller or larger distance, the electron would be reflected by the second barrier in a too low or two high position, which could lead to very long resonant snake orbits between the two barriers. Considering scattering, this will finally result in equal probabilities that the electron will be transmitted to the right or back reflected.

The separation for the largest transmission is, in this simulation, $a = 7.4\,\mu$m. In Fig. 2(a), this corresponds to the point where the center of the electron beam has reached the upper edge. Examining in some detail Fig. 5 for $B_s = 1.5\,\mathrm{T}$, one may see further very broad but small fluctuations at larger distances between barriers which might be caused by the subsequent minima and maxima that we can still see in the $\overline{\alpha}$ values; however, this is not expected to be observed in the experimental conditions, where the elastic mean free path represents a cutoff length for these effects. Other reasons can also be a cause of smearing effects. The shape of the collimated beam will be affected in the experiment by deviations from the

perfect scenario described above. For instance, diffuse scattering at imperfect edges can lead to a broadening of the emerging beam. The diffuse edge scattering limit case is presented in the right panel in Fig. 3, where random scattering takes place every time the electrons hit an edge. Although predominantly specular reflection is expected [43], even in the diffuse limit the angle range of the emerging electrons is generally preserved, while the angle distribution is flattened. Imperfections in the ferromagnetic film that creates the magnetic barrier may induce fluctuations in the magnetic barrier height or magnetic field fluctuations under the magnetic film [15]. The latter has a very small effect in the present case due to the fact that the ferromagnetic film is magnetically saturated parallel to the current direction. However, the imperfections at the edge of the ferromagnetic film may result in certain portions of the barrier of lower height. When the imperfections are so large that the magnetic barrier is open at a certain position in the y direction, some of the electrons might travel through, escaping the edge collimation and thereby smearing to some degree the effects discussed.

IV. SUMMARY AND CONCLUSIONS

The results show that the region in a two-dimensional electron gas where a closed magnetic barrier crosses the edges of a Hall bar can be regarded as a point source of a collimated electron beam. The emerging electron beam has a minimum width (standard deviation) of $\sigma_\alpha = 19.6^\circ$ for a barrier height of $B_z(0) = 0.38\,\mathrm{T}$, which is about half of the value of the injected cosine distribution and falls easily within the experimental conditions. The collimation becomes stronger with increased barrier heights and persists over a length scale which is comparable to, or even larger than, the elastic mean free path of the electron gas or, in the case where the mean free path is larger than the width of the Hall bar, until it hits the opposite edge of the electron gas. The effect was studied by simulations and demonstrated experimentally by using a second magnetic barrier as a probe. Our results represent a possible explanation for deviations between experiments with magnetic lattices and numerical simulations, where, often, edge effects are not included [32,33,44,45]. Furthermore [45], such effects may influence the performance of strain-engineered electronic circuits of graphene, where the strain acts as an effective magnetic field [37].

ACKNOWLEDGMENT

Financial support from Heinrich-Heine-University Düsseldorf is gratefully acknowledged.

[1] A. M. Song, A. Lorke, A. Kriele, J. P. Kotthaus, W. Wegscheider, and M. Bichler, Phys. Rev. Lett. **80**, 3831 (1998).
[2] B. J. van Wees, H. van Houten, C. W. J. Beenakker, J. G. Williamson, L. P. Kouwenhoven, D. van der Marel, and C. T. Foxon, Phys. Rev. Lett. **60**, 848 (1988).
[3] D. A. Wharam, T. J. Thornton, R. Newbury, M. Pepper, H. Ahmed, J. E. F. Frost, D. G. Hasko, D. C. Peacock, D. A. Ritchie, and G. A. C. Jones, J. Phys. C **21**, L209 (1988).
[4] L. W. Molenkamp, A. A. M. Staring, C. W. J. Beenakker, R. Eppenga, C. E. Timmering, J. G. Williamson, C. J. P. M. Harmans, and C. T. Foxon, Phys. Rev. B **41**, 1274 (1990).
[5] M. A. Topinka, B. J. LeRoy, S. E. J. Shaw, E. J. Heller, R. M. Westervelt, K. D. Maranowski, and A. C. Gossard, Science **289**, 2323 (2000).
[6] J. Spector, H. L. Stormer, K. W. Baldwin, L. N. Pfeiffer, and K. W. West, Appl. Phys. Lett. **56**, 1290 (1990).
[7] J. J. Heremans, S. von Molnar, D. D. Awschalom, and A. C. Gossard, Appl. Phys. Lett. **74**, 1281 (1999).
[8] H. van Houten, C. W. J. Beenakker, J. G. Williamson, M. E. I. Broekaart, P. H. M. van Loosdrecht, B. J. van Wees, J. E. Mooij, C. T. Foxon, and J. J. Harris, Phys. Rev. B **39**, 8556 (1989).
[9] A. Nogaret, J. Phys.: Condens. Matter **22**, 253201 (2010).
[10] F. M. Peeters and A. Matulis, Phys. Rev. B **48**, 15166 (1993).
[11] A. Matulis, F. M. Peeters, and P. Vasilopoulos, Phys. Rev. Lett. **72**, 1518 (1994).
[12] F. G. Monzon, M. Johnson, and M. L. Roukes, Appl. Phys. Lett. **71**, 3087 (1997).
[13] M. Johnson, B. R. Bennett, M. J. Yang, M. M. Miller, and B. V. Shanabrook, Appl. Phys. Lett. **71**, 974 (1997).
[14] V. Kubrak, A. Neumann, B. L. Gallagher, P. C. Main, M. Henini, C. H. Marrows, and B. J. Hickey, J. Appl. Phys. **87**, 5986 (2000).
[15] T. Vancura, T. Ihn, S. Broderick, K. Ensslin, W. Wegscheider, and M. Bichler, Phys. Rev. B **62**, 5074 (2000).
[16] B. L. Gallagher, V. Kubrak, A. W. Rushforth, A. C. Neumann, K. W. Edmonds, P. C. Main, M. Henini, C. H. Marrows, B. J. Hickey, and S. Thoms, Physica E (Amsterdam, Neth.) **11**, 171 (2001).
[17] V. Kubrak, K. W. Edmonds, A. C. Neumann, B. L. Gallagher, P. C. Main, M. Henini, C. H. Marrows, B. J. Hickey, and S. Thoms, IEEE Trans. Magn. **37**, 1992 (2001).
[18] M. Cerchez, S. Hugger, T. Heinzel, and N. Schulz, Phys. Rev. B **75**, 035341 (2007).
[19] A. Leuschner, J. Schluck, M. Cerchez, T. Heinzel, K. Pierz, and H. W. Schumacher, Phys. Rev. B **95**, 155440 (2017).
[20] J. Reijniers, A. Matulis, K. Chang, F. M. Peeters, and P. Vasilopoulos, Europhys. Lett. **59**, 749 (2002).
[21] A. Tarasov, S. Hugger, H. Xu, M. Cerchez, T. Heinzel, I. V. Zozoulenko, U. Gasser-Szerer, D. Reuter, and A. D. Wieck, Phys. Rev. Lett. **104**, 186801 (2010).
[22] B. Schüler, M. Cerchez, H. Xu, J. Schluck, T. Heinzel, D. Reuter, and A. D. Wieck, Phys. Rev. B **90**, 201111(R) (2014).
[23] H. Xu, T. Heinzel, M. Evaldsson, S. Ihnatsenka, and I. V. Zozoulenko, Phys. Rev. B **75**, 205301 (2007).
[24] S. Fasbender, J. Schluck, M. Cerchez, T. Heinzel, S. Sievers, K. Pierz, and H. W. Schumacher, J. Appl. Phys. **119**, 094302 (2016).
[25] A. Majumdar, Phys. Rev. B **54**, 11911 (1996).
[26] Y. Guo, B. L. Gu, Z. Zeng, J. Z. Yu, and Y. Kawazoe, Phys. Rev. B **62**, 2635 (2000).
[27] G. Papp and F. M. Peeters, Appl. Phys. Lett. **78**, 2184 (2001).
[28] G. Papp and F. M. Peeters, Appl. Phys. Lett. **79**, 3198 (2001).

[29] H. Z. Xu and Y. Okada, Appl. Phys. Lett. **79**, 3119 (2001).
[30] F. Zhai and H. Q. Xu, Appl. Phys. Lett. **88**, 032502 (2006).
[31] P. D. Ye, D. Weiss, R. R. Gerhardts, M. Seeger, K. von Klitzing, K. Eberl, and H. Nickel, Phys. Rev. Lett. **74**, 3013 (1995).
[32] H. A. Carmona, A. K. Geim, A. Nogaret, P. C. Main, T. J. Foster, M. Henini, S. P. Beaumont, and M. G. Blamire, Phys. Rev. Lett. **74**, 3009 (1995).
[33] J. Schluck, S. Fasbender, T. Heinzel, K. Pierz, H. W. Schumacher, D. Kazazis, and U. Gennser, Phys. Rev. B **91**, 195303 (2015).
[34] A. DeMartino, L. Dell'Anna, and R. Egger, Phys. Rev. Lett. **98**, 066802 (2007).
[35] H. Xu, T. Heinzel, M. Evaldsson, and I. V. Zozoulenko, Phys. Rev. B **77**, 245401 (2008).
[36] V. M. Pereira and A. H. Castro Neto, Phys. Rev. Lett. **103**, 046801 (2009).
[37] N. Levy, S. A. Burke, K. L. Meaker, M. Panlasigui, A. Zettl, F. Guinea, A. H. Castro Neto, and M. F. Crommie, Science **329**, 544 (2010).
[38] C. W. J. Beenakker and H. van Houten, Phys. Rev. B **39**, 10445 (1989).
[39] M. Cerchez and T. Heinzel, Appl. Phys. Lett. **98**, 232111 (2011).
[40] M. Büttiker, Phys. Rev. Lett. **57**, 1761 (1986).
[41] C. W. J. Beenakker, Phys. Rev. Lett. **62**, 2020 (1989).
[42] C. W. J. Beenakker and H. van Houten, Solid State Phys. **44**, 1 (1991).
[43] T. J. Thornton, M. L. Roukes, A. Scherer, and B. P. Van de Gaag, Phys. Rev. Lett. **63**, 2128 (1989).
[44] A. Nogaret, S. Carlton, B. L. Gallagher, P. C. Main, M. Henini, R. Wirtz, R. Newbury, M. A. Howson, and S. P. Beaumont, Phys. Rev. B **55**, R16037 (1997).
[45] J. F. Song, J. P. Bird, and Y. Ochiai, Appl. Phys. Lett. **86**, 062106 (2005).